Correlation of Intranodular Vascular Features with Invasiveness in Pure Ground-Glass Nodules of Lung Adenocarcinoma

Keywords
Ground-glass nodule, Angiogenesis, Invasive adenocarcinoma, Computed tomography, Artificial intelligence, Predictive model

Abstract

Introduction
This study aimed to investigate whether artificial intelligence (AI)-based quantification of intranodular vascular features on computed tomography (CT) scans can predict invasiveness in pure ground-glass nodules (pGGNs) of lung adenocarcinoma.

Material and methods
We conducted a retrospective analysis of 125 surgically resected pGGNs from 112 patients. Preoperative CT images were processed with MyrianXP-Lung software to measure nodule size (long and short diameter, volume), mean CT attenuation (Hounsfield Units, HU), and intranodular vascular volume. Pathological diagnoses were classified into minimally invasive adenocarcinoma (MIA) and invasive adenocarcinoma (IAC). Group comparisons were performed using non-parametric tests, and multivariable logistic regression was applied to identify independent predictors of IAC. Diagnostic performance was assessed using receiver operating characteristic (ROC) curves and area under the curve (AUC) values.

Results
The cohort included 68 MIA and 57 IAC cases. IAC nodules exhibited significantly larger short diameter (8.5 vs 6.1 mm, P<0.001), higher CT attenuation (-532 vs -588 HU, P<0.001), and greater vascular volume (61.2 vs 20.8 mm^3, P<0.001) compared to MIA. Multivariable analysis identified short diameter (OR=1.32, P=0.007), CT attenuation (OR=1.012, P=0.001), and vascular volume (OR=1.031, P=0.002) as independent predictors of IAC. Vascular volume showed the highest predictive accuracy (AUC=0.812), with a combined model achieving AUC=0.829. Nodule volume strongly correlated with vascular volume (r=0.905, P<0.001).

Conclusions
AI-assisted vascular volume quantification emerges as a novel predictor of invasiveness in pGGNs. Integration of vascular characteristics with radiological features provides a valuable non-invasive approach for risk stratification and personalized management, underscoring the role of angiogenesis in lung adenocarcinoma progression.

Introduction

Lung cancer remains the leading cause of cancer-related mortality worldwide [1-3]. With the adoption of low-dose CT (LDCT) screening, detection of pure ground-glass nodules (pGGNs) has increased, many of which represent early-stage lung adenocarcinoma (LUAD)[4, 5]. Pathologically, LUAD presents as a spectrum ranging from pre-invasive adenocarcinoma in situ (AIS) and minimally invasive adenocarcinoma (MIA) to invasive adenocarcinoma (IAC). Notably, AIS and MIA are associated with nearly 100% five-year recurrence-free survival after resection, whereas IAC carries a higher risk of recurrence[6, 7]. Therefore, noninvasive differentiation of IAC from AIS and MIA is clinically essential for optimizing treatment timing and strategy.

Angiogenesis is a fundamental hallmark of cancer progression[8]. In pGGNs, neovascularization supplies essential nutrients and oxygen that support tumor growth and invasion[9, 10]. Early identification and management of LUAD can be enhanced through advanced monitoring technologies such as the Artificial Intelligence of Things (AIoT), leading to more favorable outcomes[11, 12]. Notably, intranodular vascular features from CT imaging are quantifiable with advanced artificial intelligence (AI) software and may reflect the underlying tumor biology and potential for invasiveness [13-15]. Although previous studies have qualitatively assessed the relationship between vessel morphology and invasiveness[16, 17], precise quantification of intranodular vascular volume using AI remains unexplored and may offer a more objective and robust

biomarker. To that end, our study evaluated the association between intranodular vascular features on CT and pathological invasiveness in a cohort of resected pGGNs diagnosed as LUAD.

Material and methods

Study design and population

We reviewed 856 consecutive patients with GGNs who underwent surgical resection at Henan Chest Hospital between January 2019 and December 2023. The inclusion criteria were as follows: (1) age > 18 years; (2) pGGN on preoperative CT imaging (lung window: homogeneous hazy opacity without solid components, maximum diameter ≤ 30 mm); (3) availability of preoperative thin-section CT (slice thickness ≤ 1.25 mm, DICOM format); (4) pathological diagnosis of LUAD (MIA or IAC) according to the 2021 World Health Organization (WHO) criteria; and (5) no prior lung cancer treatment. Meanwhile, the exclusion criteria were as follows**:** (1) history of extrathoracic malignancy; (2) inadequate CT quality for AI segmentation; and (3) pathological diagnosis of AIS, atypical adenomatous hyperplasia (AAH), or non-adenocarcinoma. Of note, AIS was excluded to focus the analysis on the clinically important distinction between MIA and IAC, which has greater implications for surgical management. (4) Evidence of nodal or distant metastasis on preoperative staging. In total, 112 patients with 125 pGGNs met the inclusion criteria. The discrepancy between the number of patients and nodules is due to 13 patients

who each had two synchronous pGGNs, all of which were included in the analysis.

Image analysis and nodule segmentation

DICOM images were analyzed using Myrian® XP-Lung software (Intrasense, Montpellier, France). The segmentation algorithms in Myrian® XP-Lung employ advanced machine learning models trained to differentiate nodule tissue and vascular structures from the surrounding lung parenchyma based on CT attenuation and morphological characteristics. This software utilizes a combination of adaptive thresholding and region-growing algorithms, refined with morphological operations, to automatically segment the nodule and intranodular vasculature. Vascular segmentation specifically targets tubular structures based on their Hounsfield unit (HU) values and connectivity within the nodule's volume of interest. Two blinded thoracic radiologists independently performed the analyses:

Manual measurements: nodule long diameter (LD), short diameter (SD), and mean CT attenuation (measured using HU), recorded on the axial slice showing the largest cross-section of each nodule.

AI-assisted 3D quantification: The software automatically segmented the entire nodule volume and intranodular vasculature using proprietary algorithms, with manual refinement performed to ensure accurate delineation.

Nodule Volume (mm^3)

Vascular volume (mm^3) was defined as the total volume of vessels within the nodule ROI.

Vascular Volume Percentage (%) = (vascular volume/nodule volume) ×100.

Discrepancies greater than 5% were resolved by consensus.

Pathological evaluation

All specimens were processed and reviewed by experienced lung pathologists who were blinded to CT findings. Diagnoses (MIA vs. IAC) were made strictly according to the 2021 WHO classification. MIA was defined as predominantly lepidic growth with stromal invasion ≤ 5 mm in the greatest dimension. Meanwhile, IAC was defined as an invasive component lesion > 5 mm in the greatest dimension.

Statistical analysis

Statistical analyses were performed using SPSS 27.0 (IBM Corp.) and R 4.3.1. Continuous variables are presented as median (interquartile range, IQR), with comparisons between MIA and IAC groups made using the Mann-Whitney U test, while the standardized test statistic (Z-score) and *P*-values were also reported. Categorical variables are presented as frequencies (%) and compared using the Chi-square or Fisher's exact test, as appropriate. Multivariable logistic regression was used to identify independent predictors of IAC, including variables significant in univariate analysis. Multicollinearity was evaluated using variance inflation factors (VIF), with values below five indicating

no substantial multicollinearity. Model goodness-of-fit was assessed using the Hosmer-Lemeshow test. Internal validity of the combined predictive model was further evaluated using 10-fold cross-validation. Receiver operating characteristic (ROC) curves were used to assess the diagnostic performance of individual parameters and the combined model, with optimal cut-off values determined by Youden's index. Spearman correlation was used to evaluate the relationship between nodule volume and vascular volume. *P*-values < 0.05 were considered statistically significant.

Results

Clinical and pathological characteristics

The final cohort included 125 pGGNs (68 MIA, 57 IAC) from 112 patients (Table 1). There were no significant differences between the MIA and IAC groups in terms of patient age (*P* = 0.421), gender (*P* = 0.308), smoking history (*P* = 0.682), family history of cancer (*P* = 0.502), or nodule location (*P* = 0.187).

Table 1. Clinical characteristics of the study population.

Characteristics	Total (n = 125)	MIA (n = 68)	IAC (n = 57)	*P*-value
Age (years)				0.421
<60	68	39	29	
≥60	57	29	28	
Gender				0.308
Male	48	23	25	

Female	77	45	32	
Smoking History				0.682
Yes	21	11	10	
No	104	57	47	
Family History				0.502
Yes	27	13	14	
No	98	55	43	
Location				0.187
RUL	48	30	18	
RML	9	3	6	
RLL	18	8	10	
LUL	33	21	12	
LLL	17	6	11	

Abbreviations: RUL: right upper lobe, RML: right middle lobe, RLL: right lower lobe, LUL: left upper lobe, LLL: left lower lobe.

Comparison of imaging characteristics

Significant differences were observed in all quantitative CT-derived metrics between MIA and IAC nodules (Table 2; all $P < 0.001$). IAC nodules were larger (LD, SD, and volume), denser (higher CT attenuation), and exhibited significantly greater absolute vascular volume as well as a higher vascular volume percentage.

Table 2. Imaging characteristics of MIA and IAC nodules.

Variables	MIA (n = 68)	IAC (n = 57)	*Z*	*P*-value
Long Diameter (mm)	9.1 (7.0, 11.5)	13.8 (10.8, 16.5)	-5.874	<0.001
Short Diameter (mm)	6.1 (4.8, 7.6)	8.5 (7.1, 10.3)	-6.218	<0.001
CT Attenuation (HU)	-588 (-618, -555)	-532 (-569, -498)	-5.109	<0.001
Nodule Volume (mm³)	208 (132, 356)	482 (315, 872)	-6.302	<0.001
Vascular Volume (mm³)	20.8 (12.1, 35.4)	61.2 (41.5, 98.7)	-7.045	<0.001
Vascular Volume (%)	10.1% (6.8, 13.2)	12.7% (10.3, 15.8)	-4.003	<0.001

Data presented as Median (IQR). Abbreviations: Z; Standardized test statistic from the Mann-Whitney U test.

Predictors of Invasive Adenocarcinoma

Multivariable logistic regression (Hosmer-Lemeshow, $P = 0.621$, indicating good model fit) identified nodule short diameter, CT attenuation, and vascular volume as independent predictors of IAC (Table 3). Nodule volume and vascular volume percentage were excluded due to multicollinearity (VIF > 4 with vascular volume).

Table 3. Multivariable logistic regression analysis for IAC prediction.

Variables	B	SE	*P*-value	OR	95% CI
Short Diameter (mm)	0.278	0.103	0.007	1.321	1.080 - 1.616
CT Attenuation (HU)	0.012	0.004	0.001	1.012	1.005 - 1.019
Vascular Volume (mm³)	0.031	0.010	0.002	1.031	1.011 - 1.052

Abbreviations: SE: Standard Error; OR: Odds Ratio; CI: Confidence Interval.

Diagnostic Performance

ROC analysis showed good diagnostic performance for vascular volume alone (AUC = 0.812). The combined model (short diameter + CT attenuation + vascular volume) achieved the highest AUC of 0.829 (95% CI: 0.758-0.900, *P* < 0.001), with a sensitivity of 70.2% and specificity of 83.8% at the optimal cut-off (Table 4). The model demonstrated strong internal validity, with a 10-fold cross-validated AUC of 0.815.

Table 4. ROC curve analysis for predicting IAC.

Variables	AUC	Cut-off	Sensitivity	Specificity	Youden index
Short Diameter (mm)	0.761	7.25	75.4%	70.6%	0.460
CT Attenuation (HU)	0.698	-558.5	68.4%	67.6%	0.360
Vascular Volume (mm^3)	0.812	38.05	80.7%	73.5%	0.542
Combined Model	0.829	0.486	70.2%	83.8%	0.540

Correlation between nodule volume and vascular volume

Spearman correlation analysis demonstrated a very strong positive correlation between nodule volume and vascular volume across all nodules (r = 0.905, *P* < 0.001), with the relationship appearing linear across the observed size range.

Discussion

In this study of 125 resected pGGNs, quantitatively assessed intranodular vascular features on non-contrast CT proved to be promising indicators of pathological invasiveness in LUAD. Our findings solidify the critical role of

angiogenesis, as a fundamental biological driver in the progression from indolent MIA to IAC in pGGNs. The independent predictive value of nodule short diameter, CT attenuation, and vascular volume resulted in a combined model AUC of 0.829, reflecting their potential as non-invasive biomarkers for refining risk stratification and guiding clinical decision-making in this challenging patient population.

The transition of a pGGN from MIA to IAC represents a critical biological shift, characterized by the acquisition of invasive capabilities. Our observations showed that vascular volume was significantly increased within IAC nodules, marking a pivotal event in tumor progression[18-20]. In the AIS or MIA state, tumor cells predominantly grow along pre-existing alveolar structures (lepidic pattern), relying on the existing pulmonary capillary network. As genetic and epigenetic alterations accumulate (e.g., EGFR, KRAS, TP53), tumor cells and associated stromal cells, particularly cancer-associated fibroblasts (CAFs), begin to secrete a potent array of pro-angiogenic factors[21-24]. Vascular endothelial growth factor (VEGF-A), often regarded as the master regulator of angiogenesis, plays a central role [9, 25-28]. Binding of VEGFR-2 (KDR/Flk-1) on endothelial cells activates complex downstream signaling cascades, including the PI3K/Akt/mTOR pathway, which promotes endothelial cell survival, and the Ras/Raf/MEK/ERK pathway, which drives proliferation and migration[29-32]. This orchestrated response results in endothelial sprouting, tube formation, and ultimately the establishment of new, often immature and

leaky, capillaries within the developing tumor mass[33, 34]. This intratumoral neovascularization is quantified by our AI software as vascular volume. These nascent vessels supply the oxygen and nutrients necessary to support the exponential growth and metabolic demands of an expanding invasive clone. Moreover, they serve as conduits for tumor cell intravasation, representing the initial step in the metastatic cascade[35-38]. The strong correlation between nodule volume and vascular volume ($r = 0.905$, $P < 0.001$) illustrates this co-dependent relationship: tumor growth drives angiogenesis, and effective angiogenesis, in turn, facilitates further growth and invasion. These findings position angiogenesis not merely as a consequence but as an active enabler and potential biomarker of malignant progression in pGGNs.

The clinical need to accurately distinguish IAC from MIA in pGGNs is paramount. Although surgical resection provides excellent cure rates for MIA (> 95% five-year Disease-Free Survival), it carries inherent morbidity[39-41]. Conversely, delayed resection of aggressive IAC increases the risk of disease progression. Current management guidelines, including FLEISCHNER and NCCN, primarily rely on size thresholds (persistent pGGN > 6–8 mm) and interval growth as indicators for intervention or intensified surveillance[39, 42-44]. However, these parameters have significant limitations. Nodule size alone correlates poorly with invasiveness at the individual level, and growth assessment requires time, potentially delaying critical treatment in rapidly progressing cases. Integrating vascular volumetry into clinical algorithms could

reduce unnecessary surgery for benign-appearing nodules while expediting intervention for biologically aggressive lesions, thereby advancing toward truly personalized management[45]. The defined vascular volume threshold (38.05 mm^3) may serve as a practical quantitative benchmark in clinical practice. For instance, a pGGN that remains stable in size but has a vascular volume near or above this threshold may warrant closer surveillance or earlier biopsy. In contrast, a nodule with a vascular volume below this cutoff could translate to a more conservative management approach, even if its size exceeds conventional criteria, potentially reducing unnecessary surgeries. Furthermore, the vascular volume cutoff (38.05 mm^3) provides a tangible, quantifiable target for future prospective validation studies and could serve as an imaging surrogate endpoint in trials evaluating anti-angiogenic strategies for early lung cancer interception.

Quantifying complex 3D vascular structures within low-density GGNs requires sophisticated tools beyond human visual assessment. AI-powered software like Myrian® XP-Lung enables objective and reproducible volumetry, extracting features imperceptible to the naked eye, representing a significant advancement. Nonetheless, several methodological considerations warrant discussion. First, the accuracy of vascular segmentation hinges on the algorithm's ability to distinguish true intranodular vessels from subtle density fluctuations or image noise, particularly in very faint GGNs. Validation against histopathological MVD using markers such as CD31 or CD34 remains essential

but was not performed in this study[46-48]. Second, the defined ‘vascular volume’ includes both the lumen and vessel wall. While this metric correlates with perfusion capacity, it does not directly measure blood flow or vessel permeability, key hallmarks of angiogenesis. These parameters are better assessed using dynamic contrast-enhanced (DCE) CT or MR perfusion techniques, which are generally avoided in pure GGN screening due to radiation and contrast concerns. Third, the strong correlation between vascular volume and nodule volume introduced multicollinearity, necessitating careful variable selection in our regression model. Future studies could investigate more sophisticated AI-derived vascular phenotypes, such as vessel tortuosity, branching complexity (fractal dimension), or spatial distribution heterogeneity. Importantly, these may capture additional biologically relevant information independent of simple volume[49-51]. The stability of vascular volume percentage observed in larger nodules in previous studies suggests potential regulatory mechanisms or vessel co-option, representing areas for further AI-driven investigation.

Previous studies qualitatively assessed vessel changes as binary features, focusing on vessel prevalence (detection rate) and vessel volume percentage (a relative measure normalized to nodule volume), often using deep learning for segmentation[16, 17]. In contrast, the present study is the first to quantitatively and objectively measure the absolute three-dimensional volume of intranodular vasculature using dedicated, validated AI-powered software.

This approach provides a continuous, reproducible variable (vascular volume in mm^3) rather than relying on subjective morphological assessment. This methodological advancement enables a more precise and objective evaluation of angiogenesis. Using this quantitative approach, we identified vascular volume as a strong independent predictor of invasiveness (OR = 1.031, 95% CI: 1.011–1.052, P = 0.002) in multivariable analysis, alongside established features such as short diameter and CT attenuation. In contrast to Chu et al., who reported vessel changes as significant in univariate analysis but not as an independent predictor (with only mean CT attenuation and lobulation retained), our findings highlight the critical and independent role of quantitatively assessed angiogenic activity in predicting invasiveness. Our ROC analysis demonstrated that quantitatively measured vascular volume alone achieved strong diagnostic performance (AUC = 0.812), outperforming CT attenuation (AUC = 0.698) and comparable to nodule size (short diameter, AUC = 0.761). Importantly, the combined model incorporating short diameter, CT attenuation, and vascular volume yielded the highest AUC (0.829), indicating that quantitative vascular assessment provides additive diagnostic value beyond conventional size and density metrics, and markedly surpasses qualitative evaluations.

Our analysis revealed an exceptionally strong positive correlation between nodule volume and vascular volume (r = 0.905, P < 0.001). This quantitative relationship reinforces the biological paradigm that tumor expansion and

angiogenesis are tightly coupled processes. By demonstrating that larger pGGNs consistently harbor greater vascular volume, our findings provide imaging-based evidence that the growth of invasive clones is sustained by a proportional increase in blood supply, supporting a mechanistic rather than merely correlative link between angiogenesis and progression. Furthermore, the present study focused exclusively on nodules pathologically diagnosed as MIA or IAC, while excluding AAH and AIS. This focus is clinically significant, as distinguishing MIA from IAC directly informs management decisions, including the extent of surgical resection and the necessity of lymph node dissection.

While our cross-sectional study robustly demonstrates an association between vascular volume and invasiveness, longitudinal studies are still needed to determine whether acceleration in vascular volume growth precedes or coincides with the onset of histologically detectable invasion. The potential of a vascular surge to serve as an early-warning biomarker for malignant transformation in previously stable pGGNs warrants further investigation. Prospective longitudinal CT studies with precise vascular quantification are essential to map these dynamics and establish predictive thresholds. In parallel, the molecular mechanisms driving the angiogenic switch in pGGNs remain incompletely understood and require further elucidation. Integrating imaging biomarkers with genomic and proteomic profiling of resected specimens could uncover specific mutations or signaling pathway activations that underlie aggressive vascular phenotypes. Such a radiogenomic approach holds

considerable promise for building integrated diagnostic and prognostic models, bridging imaging, molecular biology, and clinical outcomes.

Another important frontier is therapeutic targeting. Elevated vascular volume, reflecting active angiogenesis and invasion, may also serve as a predictor of response to anti-angiogenic therapy. Agents such as bevacizumab (anti-VEGF-A) and VEGFR-targeting TKIs have already been established in advanced NSCLC[52]. Neoadjuvant therapy may represent a potential strategy for high-risk pGGNs identified by vascular metrics, with the aim of downstaging disease or eradicating occult micrometastases. Early-phase clinical trials exploring this paradigm are warranted. Finally, the ethical and practical integration of AI-based vascular quantification into routine screening programs requires careful consideration, particularly regarding cost, accessibility, workflow integration, and standardization across platforms and institutions.

Several limitations should be acknowledged. First, the retrospective design and exclusive inclusion of surgically resected nodules inherently introduce selection bias; Our cohort consists of nodules that were resected based on preoperative suspicion of malignancy, likely over-representing those with aggressive features relative to the broader population of screen-detected pGGNs. Second, the single-center design limits the generalizability of our findings. Third, although the sample size (n = 125 nodules) was adequate for the primary analyses and larger than many prior validation cohorts, it was insufficient for robust subgroup analyses or exploration of potential interactions between

predictors. Although internal cross-validation yielded a robust result, the model warrants validation in larger, multi-center prospective cohorts to confirm its generalizability. The absence of longitudinal follow-up data prevents assessment of how vascular features evolve over time or predict future growth and invasiveness. Additionally, pathological measurement of MVD using immunohistochemistry was not performed for direct correlation with CT-derived vascular volume, which would be a valuable addition in future prospective studies.

Conclusion

The present study confirms that nodule short diameter, CT attenuation, and intranodular vascular volume are significant independent predictors of IAC. The strong correlation between nodule volume and vascular volume reinforces the critical role of angiogenesis in tumor progression. Integrating these readily quantifiable CT features, particularly through AI-assisted vascular volumetry, offers valuable noninvasive tools for risk stratification and personalized management of patients with pGGNs.

Ethics approval and consent to participate

This retrospective single-center study was approved by the institutional review board (No. HNCH-2018-24), and informed consent was waived given the retrospective nature of this study. All procedures were conducted in accordance with the ethical standards of the institution and the Declaration of Helsinki.

Data availability

The datasets generated and analyzed during this study are available from the corresponding author upon reasonable request.

Conflict of Interest

The authors declare no conflicts of interest.

Funding

None.

References

1. Wang C, Chen B, Liang S et al. China Protocol for early screening, precise diagnosis, and individualized treatment of lung cancer. Signal Transduct Target Ther 2025; 10: 175.
2. Wagle NS, Nogueira L, Devasia TP et al. Cancer treatment and survivorship statistics, 2025. CA Cancer J Clin 2025.
3. Yu S, Yang L, Xu W et al. Analysis of tracheal, bronchial, and lung cancer attributable to respiratory system-related risk factors in 204 countries and territories from 1990 to 2019. Arch Med Sci 2024; 20: 1495-1503.
4. Deng Y, Xia L, Zhang J et al. Multicellular ecotypes shape progression of lung adenocarcinoma from ground-glass opacity toward advanced stages. Cell Rep Med 2024; 5: 101489.
5. Kim BG, Nam H, Hwang I et al. The Growth of Screening-Detected Pure Ground-Glass Nodules Following 10 Years of Stability. Chest 2025; 167: 1232-1242.
6. Liang ZR, Lv FJ, Fu BJ et al. Reticulation Sign on Thin-Section CT: Utility for Predicting Invasiveness of Pure Ground-Glass Nodules. AJR Am J Roentgenol 2023; 221: 69-78.
7. Qi L, Xue K, Li C et al. Analysis of CT morphologic features and attenuation for differentiating among transient lesions, atypical adenomatous hyperplasia, adenocarcinoma in situ, minimally invasive and invasive adenocarcinoma presenting as pure ground-glass nodules. Sci Rep 2019; 9: 14586.
8. Liu X, Zhang J, Yi T et al. Decoding tumor angiogenesis: pathways, mechanisms, and future directions in anti-cancer strategies. Biomark Res 2025; 13: 62.
9. Lee C, Kim MJ, Kumar A et al. Vascular endothelial growth factor signaling in health and disease: from molecular mechanisms to therapeutic perspectives. Signal Transduct Target Ther 2025; 10: 170.
10. Ko J, Hyung S, Heo YJ et al. Patient-derived tumor spheroid-induced angiogenesis

preclinical platform for exploring therapeutic vulnerabilities in cancer. Biomaterials 2024; 306: 122504.
11. Hsia SC, Wang SH, Chen LF, Ko BA. Real-time prediction system for prevention of acute renal failure based on AI model. Arch Med Sci 2024; 20: 2043-2050.
12. Li H, Xie T. An improved random forest algorithm for tracing the origin of metastatic renal cancer tissues. Arch Med Sci 2025; 21: 789-801.
13. Luo W, Ren Y, Liu Y et al. Imaging diagnostics of pulmonary ground-glass nodules: a narrative review with current status and future directions. Quant Imaging Med Surg 2024; 14: 6123-6146.
14. Yang Y, Xu J, Wang W et al. Meta-analysis of the correlation between CT-based features and invasive properties of pure ground-glass nodules. Asian J Surg 2023; 46: 3405-3416.
15. Wu L, Gao C, Kong N et al. The long-term course of subsolid nodules and predictors of interval growth on chest CT: a systematic review and meta-analysis. Eur Radiol 2023; 33: 2075-2088.
16. Chu ZG, Li WJ, Fu BJ, Lv FJ. CT Characteristics for Predicting Invasiveness in Pulmonary Pure Ground-Glass Nodules. AJR Am J Roentgenol 2020; 215: 351-358.
17. Zhao B, Wang X, Sun K et al. Correlation Between Intranodular Vessels and Tumor Invasiveness of Lung Adenocarcinoma Presenting as Ground-glass Nodules: A Deep Learning 3-Dimensional Reconstruction Algorithm-based Quantitative Analysis on Noncontrast Computed Tomography Images. J Thorac Imaging 2023; 38: 297-303.
18. Bergers G, Benjamin LE. Tumorigenesis and the angiogenic switch. Nat Rev Cancer 2003; 3: 401-410.
19. Ribatti D, Nico B, Crivellato E et al. The history of the angiogenic switch concept. Leukemia 2007; 21: 44-52.
20. Baeriswyl V, Christofori G. The angiogenic switch in carcinogenesis. Semin Cancer Biol 2009; 19: 329-337.
21. Zhang C, Zhang J, Xu FP et al. Genomic Landscape and Immune Microenvironment Features of Preinvasive and Early Invasive Lung Adenocarcinoma. J Thorac Oncol 2019; 14: 1912-1923.
22. Qian J, Zhao S, Zou Y et al. Genomic Underpinnings of Tumor Behavior in In Situ and Early Lung Adenocarcinoma. Am J Respir Crit Care Med 2020; 201: 697-706.
23. Nie M, Yao K, Zhu X et al. Evolutionary metabolic landscape from preneoplasia to invasive lung adenocarcinoma. Nat Commun 2021; 12: 6479.
24. Hu X, Fujimoto J, Ying L et al. Multi-region exome sequencing reveals genomic evolution from preneoplasia to lung adenocarcinoma. Nat Commun 2019; 10: 2978.
25. Shaposhnikov M, Thakar J, Berk BC. Value of Bioinformatics Models for Predicting Translational Control of Angiogenesis. Circ Res 2025; 136: 1147-1165.
26. Shin S, Choi Y, Jang W et al. A vascularized tumors-on-a-chip model for studying tumor-angiogenesis interplay, heterogeneity and drug responses. Mater Today Bio 2025; 32: 101741.
27. Shah FH, Nam YS, Bang JY et al. Targeting vascular endothelial growth receptor-2 (VEGFR-2): structural biology, functional insights, and therapeutic resistance. Arch Pharm Res 2025; 48: 404-425.

28. Li J, Li Z, Wang K. Targeting angiogenesis in gastrointestinal tumors: strategies from vascular disruption to vascular normalization and promotion strategies angiogenesis strategies in GI tumor therapy. Front Immunol 2025; 16: 1550752.
29. Queisser A, Seront E, Boon LM, Vikkula M. Genetic Basis and Therapies for Vascular Anomalies. Circ Res 2021; 129: 155-173.
30. Stefani C, Miricescu D, Stanescu S, II et al. Growth Factors, PI3K/AKT/mTOR and MAPK Signaling Pathways in Colorectal Cancer Pathogenesis: Where Are We Now? Int J Mol Sci 2021; 22.
31. Laha D, Nilubol N, Boufraqech M. New Therapies for Advanced Thyroid Cancer. Front Endocrinol (Lausanne) 2020; 11: 82.
32. Claesson-Welsh L, Welsh M. VEGFA and tumour angiogenesis. J Intern Med 2013; 273: 114-127.
33. Kong M, Zhai Y, Liu H et al. Insights into the mechanisms of angiogenesis in hepatoblastoma. Front Cell Dev Biol 2025; 13: 1535339.
34. Wiśniewska W, Kopka M, Siemiątkowska K et al. The complexity of tumour angiogenesis based on recently described molecules. Contemp Oncol (Pozn) 2021; 25: 33-44.
35. Chaplain MA, McDougall SR, Anderson AR. Mathematical modeling of tumor-induced angiogenesis. Annu Rev Biomed Eng 2006; 8: 233-257.
36. Chiang SP, Cabrera RM, Segall JE. Tumor cell intravasation. Am J Physiol Cell Physiol 2016; 311: C1-c14.
37. Borriello L, Karagiannis GS, Duran CL et al. The role of the tumor microenvironment in tumor cell intravasation and dissemination. Eur J Cell Biol 2020; 99: 151098.
38. Deryugina EI, Quigley JP. Tumor angiogenesis: MMP-mediated induction of intravasation- and metastasis-sustaining neovasculature. Matrix Biol 2015; 44-46: 94-112.
39. Travis WD, Brambilla E, Noguchi M et al. International association for the study of lung cancer/american thoracic society/european respiratory society international multidisciplinary classification of lung adenocarcinoma. J Thorac Oncol 2011; 6: 244-285.
40. Fang W, Xiang Y, Zhong C, Chen Q. The IASLC/ATS/ERS classification of lung adenocarcinoma-a surgical point of view. J Thorac Dis 2014; 6: S552-560.
41. Zhang Y, Ma X, Shen X et al. Surgery for pre- and minimally invasive lung adenocarcinoma. J Thorac Cardiovasc Surg 2022; 163: 456-464.
42. Hatabu H, Hunninghake GM, Richeldi L et al. Interstitial lung abnormalities detected incidentally on CT: a Position Paper from the Fleischner Society. Lancet Respir Med 2020; 8: 726-737.
43. Farjah F, Monsell SE, Smith-Bindman R et al. Fleischner Society Guideline Recommendations for Incidentally Detected Pulmonary Nodules and the Probability of Lung Cancer. J Am Coll Radiol 2022; 19: 1226-1235.
44. Wood DE, Kazerooni EA, Baum SL et al. Lung Cancer Screening, Version 3.2018, NCCN Clinical Practice Guidelines in Oncology. J Natl Compr Canc Netw 2018; 16: 412-441.

45. Xie X, Heuvelmans MA, van Ooijen PM et al. A practical approach to radiological evaluation of CT lung cancer screening examinations. Cancer Imaging 2013; 13: 391-399.
46. Uzzan B, Nicolas P, Cucherat M, Perret GY. Microvessel density as a prognostic factor in women with breast cancer: a systematic review of the literature and meta-analysis. Cancer Res 2004; 64: 2941-2955.
47. Bais C, Mueller B, Brady MF et al. Tumor Microvessel Density as a Potential Predictive Marker for Bevacizumab Benefit: GOG-0218 Biomarker Analyses. J Natl Cancer Inst 2017; 109.
48. Raica M, Cimpean AM, Ribatti D. Angiogenesis in pre-malignant conditions. Eur J Cancer 2009; 45: 1924-1934.
49. Gillies RJ, Brown JS, Anderson ARA, Gatenby RA. Eco-evolutionary causes and consequences of temporal changes in intratumoural blood flow. Nat Rev Cancer 2018; 18: 576-585.
50. Yang J, Dong X, Jin S et al. Radiomics Model of Dynamic Contrast-Enhanced MRI for Evaluating Vessels Encapsulating Tumor Clusters and Microvascular Invasion in Hepatocellular Carcinoma. Acad Radiol 2025; 32: 146-156.
51. Han S, Stoyanova R, Lee H et al. Automation of pattern recognition analysis of dynamic contrast-enhanced MRI data to characterize intratumoral vascular heterogeneity. Magn Reson Med 2018; 79: 1736-1744.
52. Rosell R, Pedraz-Valdunciel C. Are neutralising anti-VEGF or VEGFR2 antibodies necessary in the treatment of EGFR-mutated non-small-cell lung cancer? Lancet Oncol 2019; 20: 1617-1618.

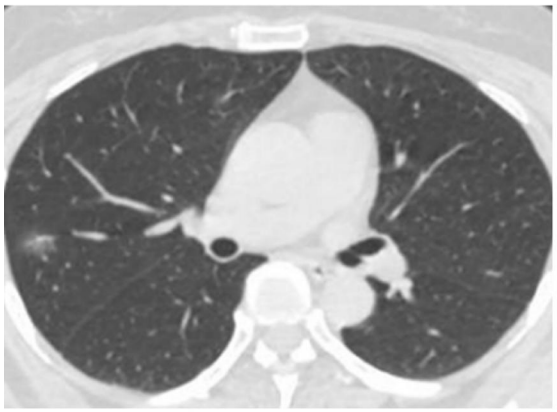

This graphical abstract summarizes the study evaluating AI-assisted quantification of intranodular vascular features for predicting invasiveness in pure ground-glass nodules (pGGNs). The study retrospectively analyzed 125 pGGNs (68 minimally invasive adenocarcinoma [MIA] and 57 invasive adenocarcinoma [IAC]) using MyrianXP-Lung software. Key findings demonstrated that IAC nodules had significantly larger short diameter, higher CT attenuation, greater volume, and notably larger vascular volume compared to MIA nodules. Multivariable analysis identified these three factors as independent predictors of IAC. Receiver operating characteristic (ROC) curve analysis showed that vascular volume had the highest individual predictive power (AUC=0.812), and a combined model achieved superior performance (AUC=0.829). The strong correlation between nodule volume and vascular volume suggests active angiogenesis. The conclusion highlights that the AI-based assessment of intranodular vascular volume provides a novel, non-invasive tool for improving risk stratification and guiding personalized management plans for patients with pGGNs.